Quantification of collagen fiber orientation based on center line of second harmonic generation image for naturally aging skins*

LI Zhi-fang (李志芳)**, QIU Shao-ping** (邱少平)**, WU Shu-lian** (吴淑莲)**, and LI Hui** (李晖)**

Key Laboratory of Optoelectronic Science and Technology for Medicine, Ministry of Education, Fujian Provincial Key Laboratory of Photonic Technology, Fujian Provincial Engineering Technology Research Center of Photoelectric Sensing Application, College of Photonic and Electronic Engineering, Fujian Normal University, Fuzhou 350007, China

(Received 10 February 2018; Revised 25 April 2018)

Quantification of fiber orientation is the key to characterizing the tissue mechanical properties and diagnosing diseases. A center line-based algorithm is presented for estimating the orientation distribution that first skeletonizes a binary image of fibers, followed by orientation estimation using a weight vector summation algorithm along the center line of image. Then we use the orientation at the skeleton to approximate the orientation of each pixel between the boundary and skeleton. The algorithm is applied for characterizing collagen fibers of mouse skins in second harmonic generation (SHG) image, and the circle standard deviation of orientation could be a biomarker to differentiate the naturally aging skins.

Document code: A **Article ID:** 1673-1905(2018)04-0306-5

DOI https://doi.org/10.1007/s11801-018-8023-z

Collagen is a main structural protein in the extracellular space in various connective tissues in animal bodies and the most abundant protein in mammals[1], making up from 25% to 35% of total protein content. Collagen is in the form of elongated fibrils and mostly found in fibrous tissues such as skin[2]. Measurement of fiber orientation could accurately predict mechanical properties using a variety of microstructural models of tissue biomechanics[3]. In addition, fiber orientation distribution could be a potential biomarker for diagnosing tumor[4], myocardial infarction[5], and aging skin[2].

A number of approaches have been widely applied to quantify the average fiber direction in an image. One is based on the fast Fourier transform (FFT)[2,5-8]. A two-dimensional (2-D) power spectral density (PSD) image was employed to accurately measure the average fiber orientation distribution based on discrete Fourier transform[7,8]. And some other indirect parameters such as the ratio of short axis to long axis of logarithmic PSD images[2] and angle entropy[5] were presented for quantitative information of fiber arrangement. However, the FFT-based techniques generally require a square sub-image size and are prone to produce systematic measurement errors when the sub-image does not contain fibers.

In addition, fiber orientation could be estimated by calculating arctangent of the x and y gradient values at each pixel using the edge detection algorithm[9-12]. However, this approach requires manual threshold to identify windows with no fiber tissue, and it also requires empirical threshold of confidence value for fiber orientation determined by normality test[9]. And in regions of no intensity variation, this method might induce some errors. Thus, this method generally suffers from inaccuracy that makes it hard for quantifying exact fiber orientation.

The goal of this study is to develop an algorithm for accurate quantification of fiber orientation at each pixel within an image without knowing fiber size in prior. This algorithm is based on the center line image. The weight vector summation algorithm[13-15] is employed for estimation of skeletonized fiber. Then the local orientation of skeletonized fiber is combined with the corresponding fiber size to characterize the region of fiber orientation. The accuracy of this algorithm is evaluated by simulated images with known orientations. After validation, this technique is used to characterize naturally aging skins in second harmonic generation (SHG) images.

Fig.1 shows the overall flowchart of extracting quantitative information of fiber orientation. We use two-dimensional Otsu's threshold[16] to generate the binary image and segment the fiber bundles. Then the binary image of fiber bundles shrinks to a center line based on the thinning algorithm[17] and becomes a skeletonized image, since thinning transformation keeps topologically

* This work has been supported by the National Natural Science Foundation of China (Nos.81571726 and 61675043).

** E-mail: hli@fjnu.edu.cn

equivalent features such as position. Finally, a weighted orientation vector summation algorithm[13-15] is applied for detecting orientation of fiber skeleton and fiber size distribution is used to measure the probability density of fiber orientation.

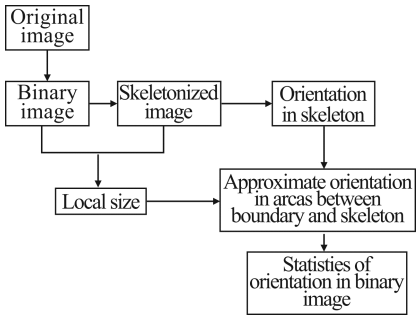

Fig.1 Flowchart of extracting quantitative information of fiber orientation

The direction α of the window center (N+1, N+1) is determined by the weighted circular mean of all direction candidates in a small square window of (2N+1)×(2N+1) as given by[13-15]:

$$\alpha = \arg\left(\sum_{j=1}^{N\times N} w_j \cdot \exp(i\alpha_j)\right) , \quad (1)$$

where $N\times N$ is the number of directions around the center, the weight w_j is inverse of their distance L from the center point and the lack of variance in binary intensity I (0 or 1) among the points, and $w_j=w_i\times w_d$, where $w_i = \sqrt{1/3} - \sqrt{\sum_{k=1}^{3}\left(I_k - \bar{I}\right)^2/2}$, and $w_d=1/L$. All values are in the range from 0° to 180°. The mean of orientation is calculated based on the circle statistics[18]. Then, the center line image times orientation image to extract the orientation at the skeleton.

The size of fiber can be quantified by the parameter of radius. The local radius for every pixel (s) on the skeleton is defined as the minimal distance between the skeleton and pixel b on the boundary set (B) in the binary image as shown in Fig.2.

$$R(b) = \min_{b\in B}[dist.(s,b)] \quad . \quad (2)$$

For pixels located between the boundary and the skeleton, the orientations are approximated as that the corresponding orientation at the point S is extracted in skeletonized image. Thus, the orientations between boundary and skeleton are equal and the number of orientation is approximated as the areas between boundary and skeleton, which can be given by $R\times L$, where L is pixel size. When the skeleton set s is in the ends of skeleton, the number of orientations is approximated as $\pi R_a^2/2$, where R_a is the radius at the ends of skeleton. Thus, we use the orientation at the skeletonized image combining with the number distribution of the corresponding orientation for quantifying the orientation distribution in the whole image. The probability density function is estimated from histogram of spatially-resolved orientation image ranging from 0° to 180°, and statistical parameters including the mean and the standard deviation of orientation are calculated.

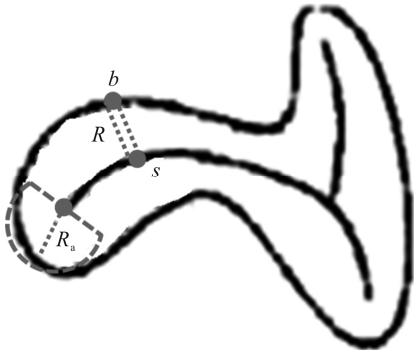

Fig.2 The relationship between the boundary and skeleton

SHG, as previously described[2], is equipped with a Plan-Neofluar (20×, *NA* = 0.4) objective. The excitation wavelength at 810 nm is used with an average power of about 8 mW. The signal is detected through a 388—420 nm IR band-pass filter. The image size is 460.68 μm×460.68 μm with 512 pixels×512 pixels. *In vivo* studies are performed using Kun-Ming mice around 20 g to 28 g. Kun-ming mice with ages of 16 weeks (young statue) and 60 weeks (old statue), respectively, are chosen to be imaged in SHG. The SHG images of dermal structure at the depth of 48 μm are detected for each mouse *in vivo*.

The circle statistics are applied for analyzing the mean and the standard deviation of orientations is calculated based on the probability density function of orientation ranging from 0° to 180°[18]. A Watson-Williams two-sample test[18] is used to determine whether the difference is significant in the statistical parameters of orientation.

To quantitatively assess the accuracy of the orientation calculation algorithm, we apply this algorithm to calculate the orientation of a simulated circle image as shown in Fig.3(a). The corresponding center lines are extracted from the binary image as shown in Fig.3(b). Then, a window size of 5×5 is applied for estimating fiber orientation along the center line using the weighted orientation vector summation algorithm. Fig.3(c) shows the spatially-resolved orientation image of the center line. The orientation image [Fig.3(c)] is combined with the number distribution of the corresponding orientation [Fig.3(d)] to generate the probability density function of orientation in the image. In addition, errors of their means of orientation for different widths of circle depend on window size. The minimum errors for different widths are estimated at the various window sizes. However, the errors for different widths estimated at the window size of 15 pixels×15 pixels [region D in Fig.4] are less than 1°, and their values approximately equal each other among three values. Thus, the computer algorithm for orientation estimation based on window size of

15 pixels×15 pixels is independent of fiber width, and is reliable for extracting fiber orientation.

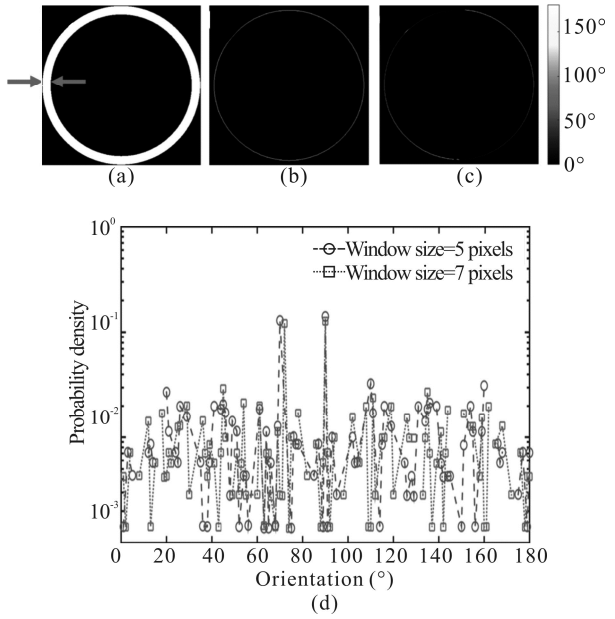

Fig.3 (a) Simulated circle image with width of 24 pixels labeled with two arrows; (b) The corresponding center line; (c) Orientation image of the center line estimated by the weighted orientation vector summation algorithm based on the window size of 5 pixels ×5 pixels; (d) Probability density of orientation

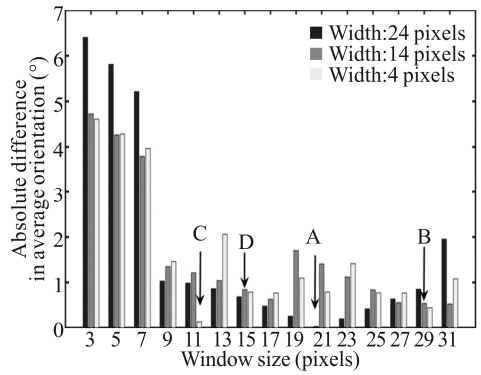

Fig.4 Errors in simulated circle orientation measurements with respect to circle width and window size used for the vector summation measurements (The minimums in circle with widths of 24 pixels, 14 pixels and 4 pixels are at the window sizes of (A) 21×21, (B) 29×29 and (C) 11×11, respectively. The theoretical mean of orientation in circle is 90°. Errors in the region D are less than 1°.)

To assess the applicability of this algorithm, fiber alignment distributions are calculated from SHG image of collagen fiber. Fig.5 is processed following the flowchart as shown in Fig.1 to extract the fiber orientation. Fig.5(a) shows SHG grayscale image of collagen fiber in mouse skin. Fig.5(b) indicates the fiber bundles are segmented based on the two-dimensional Otsu's threshold. Fig.5(c) and (d) are the center line and the orientation map, respectively. The probability density of orientation from Fig.5(e) demonstrates main component of orientation distribution in the range from ~90° to ~135°. The standard deviations of orientations are calculated based on the probability density function of orientation, and there is significant difference in skins at young and old stages as shown in Fig.6. A smaller standard deviation of orientation means that collagen fibers are more highly oriented and organized. The results indicate that the collagen alignment becomes more oriented and organized with natural aging.

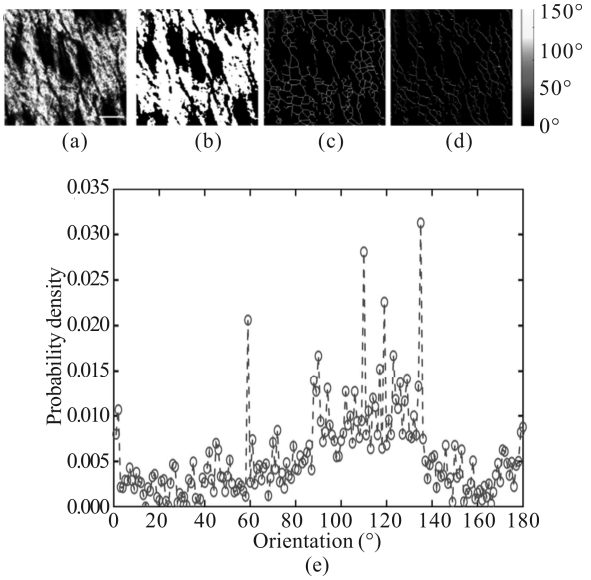

Fig.5 (a) SHG image of collagen fiber of mouse skin with 16 weeks aging; (b) Binary image; (c) The corresponding center line; (d) Orientation image of the center line; (e) Probability density of orientation (Scalebar: 100 μm)

In this work, orientation is estimated by weighted orientation vector summation algorithm based on the center line image, which is different from the algorithm for image. Fig.7(a), (b) and (c) demonstrate that the orientation is related to the window size used for weighted orientation vector summation algorithm for binary circle image, especially for the regions of A and B. This is because there is no intensity fluctuation in regions A and B, which induces the intensity variation equals zero. In order to remove orientation in the region A, the orientation image is multiplying binary circle image, as shown in Fig.7(d), (e) and (f). In addition, Fig.7(d), (e) and (f) indicate that the orientations at the boundary, such as the point C, are approximately equal, which demonstrates the advantage of boundary used for the weighted orientation vector summation algorithm.

Furthermore, the edge detection is employed for estimating the orientation based on the intensity variation in *x*- and *y*-directions[9-11]. It is suitable to calculate orientation of boundary C in image as shown in Fig.8. However, if there is no intensity variation in the interior of a fiber,

such as the region of interest (ROI) A and ROI B in Fig.8, the orientation is estimated as 0°, which is a large error. Thus, we present the skeletonized image applied for the weighted orientation vector summation algorithm to make full use of advantage of boundary, since the center lines are all boundaries.

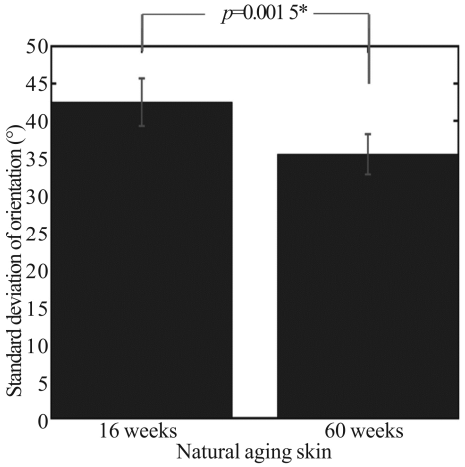

Fig.6 Standard deviation of fiber orientation on different aging skins (* denotes significant difference.)

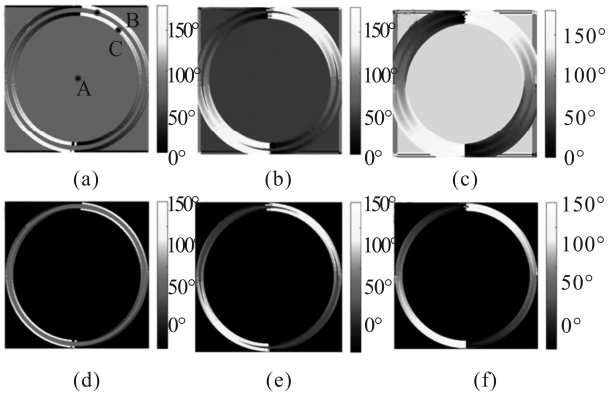

Fig.7 Orientation images of simulated binary circle images with width of 24 pixels calculated by weighted orientation vector summation algorithm based on the window sizes of (a) 3×3, (b) 11×11 and (c) 21×21, respectively; (d) (e) (f) Orientation images multiplying the corresponding binary circle images for (a), (b) and (c), respectively (A is in the region without circle, B is in the circle, and C is at the boundary.)

In this work, the statistical parameters including the mean and standard deviation of orientations are calculated based on the probability density function of orientation ranging from 0° to 180°. However, the mean of orientation depends on the rotation angle of image as shown Fig.9, which means that the mean of orientation is related to the direction of sample placement. The standard deviation of orientation is independent of the rotation angle. Thus, the standard deviation is applied for characterizing the naturally aging skins due to the result of Fig.6.

In this study, the standard deviation of orientation can differentiate the morphology of collagen fiber in different naturally aging skins, which is consistent with orientation index calculated by the ratio of short axis to long axis of Fourier transformed image[2]. However, an empirical threshold is required for binary image of FFT amplitude image, as shown in Fig.10. Furthermore, ellipse coverage of the binary FFT image is a manual process. The thresholding value of 146 is set to binarize the FFT image. Then an ellipse is chosen manually to cover the binary image of FFT image, and the short axis and long axis are calculated. Thus, the orientation index calculated by the ratio of short axis to long axis uses a semi-automatic algorithm, which might be prone to manual errors. The standard deviation of orientation is better than the orientation index for characterizing collagen fiber in the naturally aging skins.

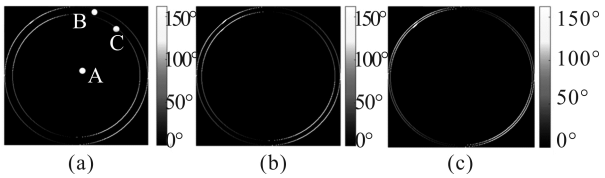

Fig.8 Orientation images of simulated binary circle images with various widths of (a) 24 pixels, (b) 14 pixels and (c) 4 pixels calculated by Sobel edge detection

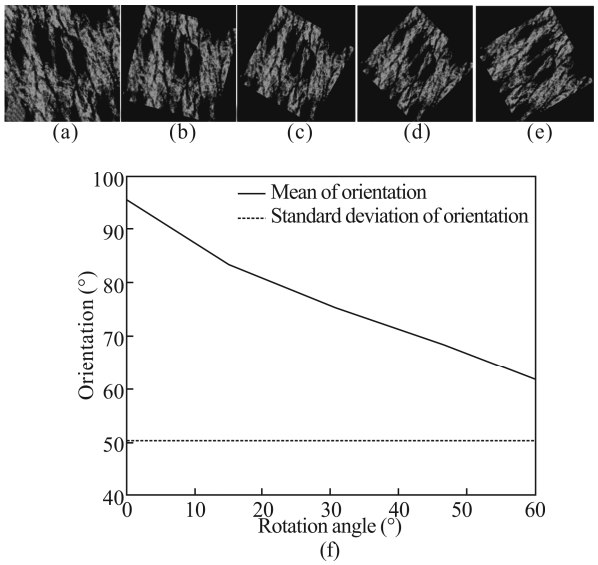

Fig.9 SHG images of collagen fiber at different rotation angles: (a) 0°, (b) 15°, (c) 30°, (d) 45°, and (e) 60°; (f) Mean and standard deviation of fiber orientation vs. rotation angle

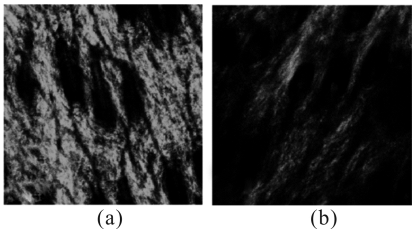

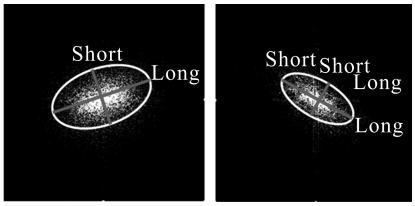

Fig.10 SHG images of collagen structure at different aging models: (a) 16 weeks and (b) 60 weeks; Corresponding binary images of FFT for (a) and (b), respectively. (FFT was performed in ImageJ software, and the level threshold was set as 146.)

In summary, we present a center line-based algorithm for determination of fiber orientation. The computer algorithm employs the weighted orientation vector summation algorithm based on center line of fiber. And by approximating that the orientations are equal at each pixel between the boundary and skeleton, the orientation distribution of an image is estimated. The accuracy of algorithm is independent of fiber width. This algorithm is applied for characterizing collagen fibers of SHG images of mouse skins. The results demonstrate that the standard deviation of orientation could distinguish the morphology of collagen fiber in young and old aging skins. Beside SHG, the center line-based algorithm of fiber orientation can be applied for other imaging modalities, including light microscopy[4], polarized light imaging[11], and scanning electron microscopy[19]. The center line-based algorithm can produce pixel-wise orientation data and enables a wider variety of diagnostic metrics based on the spatially-resolved orientation distribution image.

References

[1] L.G. Di, S.M. Sweeney, J. Korkko, L. Ala-Kokko and J.D. San Antonio, Journal of Biological Chemistry **277**, 4223 (2002).

[2] S. Wu, H. Li, H. Yang, X. Zhang, Z. Li and S. Xu, Journal of Biomedical Optics **16**, 040502 (2011).

[3] G. Chagnon, M. Rebouah and D. Favier, Journal of Elasticity **120**, 129 (2015).

[4] H. Majeed, C. Okoro, A. Kajdaccsy-Balla and K.C. Toussaint Jr., Journal of Biomedical Optics **22**, 46004 (2017).

[5] C.J. Goergen, H.H. Chen, S. Sakadžić, V.J. Srinivasan and D.E. Sosnovik, Physiological Reports **4**, e12894 (2016).

[6] R.A. Rao, M.R. Mehta and K.C. Toussaint Jr., Optics Express **17**, 14534 (2009).

[7] C. Bayan, J.M. Levitt, E. Miller, D. Kaplan and I. Georgakoudi, Journal of Applied Physics **105**, 102042 (2009).

[8] C.J. Goergen, H. Radhakrishnan, S. Sakadzic, E.T. Mandeville, E.H. Lo, D.E. Sosnovik and V.J. Srinivasan, Optics Letters **37**, 3882 (2012).

[9] C.P. Fleming, C.M. Ripplinger, B. Webb, I.R. Efimov and A.M. Rollins, J. Biomed. Opt. **13**, 030505 (2008).

[10] Y. Gan and C.P. Fleming, Biomedical Optics Express **4**, 2150 (2013).

[11] Y. Wang, K. Zhang, N.B. Wasala, X. Yao, D. Duan and G. YAO, Biomedical Optics Express **5**, 2843 (2014).

[12] C.M. Ambrosi, V.V. Fedorov, R.B. Schuessler, A.M. Rollins and I.R. Efimov, Journal of Biomedical Optics **17**, 071309 (2012).

[13] K.P. Quinn and I. Georgakoudi, Journal of Biomedical Optics **18**, 046003 (2013).

[14] W. Yao, Y. Gan, K.M. Myers, J.Y. Vink, R.J. Wapner and C.P. Hendon, Plos One **11**, e0166709 (2016).

[15] Zhiyi Liu, K.P. Quinn, L. Speroni, L. Arendt, C. Kuperwasser, C. Sonnenschein, A.M. Soto and I. Georgakoudi, Biomedical Optics Express **6**, 2294 (2015).

[16] J. Liu, W. Li and Y. Tian, Automatic Thresholding of Gray-level Pictures Using Two-dimension Otsu Method, International Conference on Circuits and Systems, 325 (1991).

[17] L. Lam, S.W. Lee and C.Y. Suen, IEEE Transactions on Pattern Analysis & Machine Intelligence **14**, 869 (1992).

[18] P. Berens, Journal of Statistical Software **31**, 1 (2009).

[19] L. Pannarale, P. Braidotti, L. d'Alba and E. Gaudio, Acta Anatomica **151**, 36 (1994).